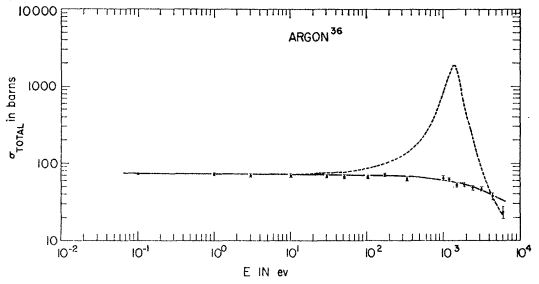

FIG. 1. This figure shows a plot of σ_{total} for Ar^{36} versus incident neutron energy. Points are measured cross sections, while the solid curve is the one calculated with negative-energy resonance, with parameters as given in the text. Dotted curve is the cross section calculated on the basis of a positive-energy resonance and is in disagreement with the data.

isotope diffusion group at Yale. The isotopic analysis of the sample is given in Table I.

The total sample thickness was 6.72×10^{21} atoms/cm^2, obtained by condensing 72.8 ± 0.7 cc of gas (measured at STP) into the sample holder, of internal dimensions $2.05\times2.75\times0.1$ cm. The thick walls of the holder, necessary for confining the gas at high pressure, produced a beam loss of some 40%.

The sample was run at one slit of the BNL fast chopper at speeds ranging from 388 to 10 000 rpm in order to cover an energy range from 0.1 ev to 6 kev. The transmission was obtained by cycling a similar, empty holder with the one containing the argon gas. A later measurement established that the sample holder and dummy holder were identical to 1% with regard to wall thickness in the beam. After small corrections for the other gases in the sample, a cross section for Ar^{36} was obtained. Figure 1 shows the data points in the region from 0.1 ev to 6 kev. A decreasing cross section is clearly seen.

III. RESULTS AND DISCUSSION

Previous work on Ar^{36} include the studies of Henshaw[1] and work by McMurtrie and Crawford.[5] Henshaw found, at 0.076 ev, a total cross section of 77 ± 9 barns. Extrapolation of the present data below 0.1 ev gives a value of 74 ± 11 barns, in agreement with Henshaw's measurement. McMurtrie and Crawford have measured the absorption cross section for Ar^{36} with pile neutrons. At 0.076 ev their measurement implies a capture cross section of 4 barns. These previous measurements, when combined with an estimated radius parameter, R', of 4.5 fermis, can be satisfied by either one of a pair of resonances, one at positive, the other at a negative energy. Figure 1 shows that the positive energy choice is ruled out by the present experiment. The statistical errors on the data points of Fig. 1 range from 2.6% at 0.1 ev to 7% at 3 kev. There is present, however, an additional systematic error of 14% which reflects uncertainties in sample thickness, which are aggravated by the relative thinness of the sample ($T\approx0.8$) over most of the energy range covered.

The solid curve through the data points was obtained from the following best fit parameters in the Breit-Wigner single-level formula:

$$E_0=-9.8\pm1.0 \text{ kev},$$
$$\Gamma_n^0=82\pm10 \text{ ev},$$
$$\Gamma_\gamma=1.85\pm0.22 \text{ ev}.$$

ACKNOWLEDGMENTS

The authors are indebted to Professor W. W. Watson and Mr. Martin Wain of Yale University for the cooperation in making available the sample of Ar^{36}.

[5] G. E. McMurtrie and D. P. Crawford, Phys. Rev. 77, 840 (1950).

PHYSICAL REVIEW VOLUME 125, NUMBER 1 JANUARY 1, 1962

Elastic Scattering of 24-Mev Neutrons by Al, Fe, Sn, Bi†

T. P. STUART, J. D. ANDERSON, AND C. WONG
Lawrence Radiation Laboratory, University of California, Livermore, California

(Received July 12, 1961)

Angular distributions have been measured for angles between 15° and 90° in 5° steps. Cylindrical scatterers were $\frac{1}{2}$ or $\frac{3}{4}$ mean-free path in diameter as calculated on the basis of total cross sections. These cylinders were bombarded with neutrons from the $T(d,n)He^4$ reaction, and the scattered neutrons were detected in a plastic scintillator. Biases were set at energies between 14 and 24 Mev. Corrections for effects due to scatterer size were calculated with a Monte Carlo code on the Univac and IBM 704. The corrected cross sections are in good agreement with optical model calculations by Bjorklund and Fernbach.

I. INTRODUCTION

THE validity of an optical model description of the nucleon-nucleus interaction is well established. Of primary interest now are the features of this potential, such as spatial extent, shape and magnitude, and the dependence of the parameters on the energy of the incident nucleon. The energy dependence of the potential is of particular interest because the saturation property of nucleon binding energy inside a nucleus requires that the potential be velocity dependent. Both

† This work was performed under the auspices of the U. S. Atomic Energy Commission.

neutron and proton data are interesting because the neutron excess in stable nuclei indicates a difference between the neutron-nucleus potential and the nuclear part of the proton-nucleus potential.

Existing measurements of neutron elastic-scattering angular distributions,[1–5] neutron nonelastic cross sections,[6–9] and total cross sections[10–14] are sufficient for a reasonably thorough study of optical model parameters for incident energies below 15 Mev, and parameters have been fairly well determined. Neutron elastic-scattering angular distributions have not been measured for incident energies between 15 and 84 Mev. As an aid to a better determination of optical model parameters at an intermediate energy, it was felt that neutron elastic-scattering angular distributions for a representative group of elements should be measured at 24 Mev. These distributions complement existing measurements of total cross sections[15] and neutron nonelastic cross sections[16] in this energy region.

II. METHOD

A. Geometry

The experimental geometry is sketched in Fig. 1. Deuterons, accelerated to 7.7 Mev by the Livermore variable-energy cyclotron, were incident on a 2.5-cm-diameter, 10-cm-long gas target filled to slightly less than 1 atmosphere of tritium. The tantalum entrance foil on the gas target had a thickness of 17 mg/cm^2. Typical beams of 8 μa on the target yielded 10^8 neutrons per steradian per second at zero degrees to the deuteron beam.

Cylindrical scatterers were placed 110 cm from the target at zero degrees to the deuteron beam. The scatterers were either $\frac{1}{2}$ or $\frac{3}{4}$ total mean-free path in diameter and were about 20-cm long. Background runs were made at each scattering angle with an empty scatterer holder positioned as during the "scatterer in" runs.

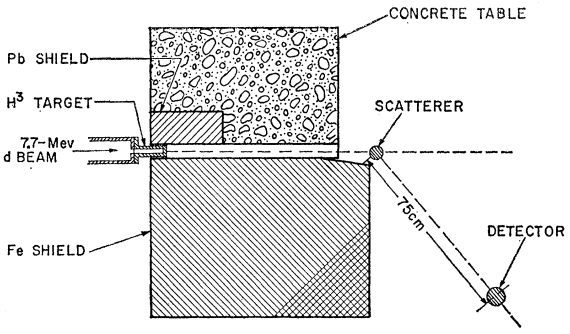

FIG. 1. Schematic diagram of experimental geometry.

Neutrons were detected in a plastic scintillator 5 cm in diameter and 7-cm long. The scintillator was located in the horizontal plane containing the gas target on a 75-cm radius from the axis of the scattering cylinder. The RCA-6655 A photomultiplier viewing the scintillator was enclosed in a metal pipe to shield against magnetic fields, and the pipe was wound with cooling coils to stabilize photomultiplier temperature and maintain constant gain. The detector was shielded from the direct source neutrons by a slab of Fe.

An identical scintillator system located in an unshielded position about 3 meters from the neutron source and a few degrees from the deuteron beam line was used to monitor neutron production. Both monitor and detector systems were biased at identical energies on their recoil spectra in order to minimize efficiency changes due to small changes in energy of the source neutrons.

B. Electronics

A block diagram of the detector electronics is shown in Fig. 2. The signal from the photomultiplier was fed

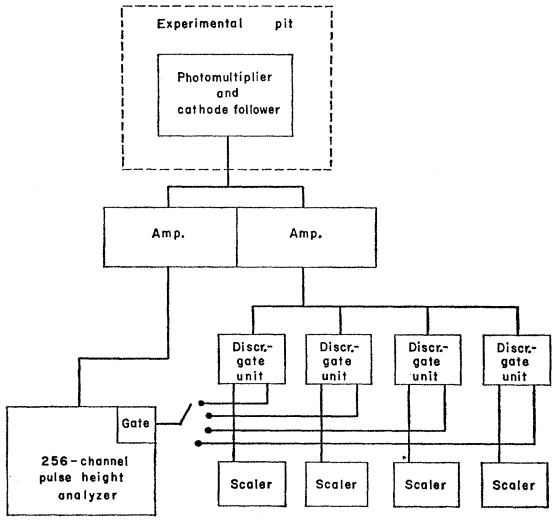

FIG. 2. Block diagram of electronics.

[1] M. Walt and H. H. Barschall, Phys. Rev. **93**, 1062 (1954).
[2] M. Walt and J. R. Beyster, Phys. Rev. **98**, 677 (1955).
[3] J. H. Coon, R. W. Davis, H. E. Felthauser, and D. B. Nicodemus, Phys. Rev. **111**, 250 (1958).
[4] M. P. Nakada, J. D. Anderson, C. C. Gardner, and C. Wong, Phys. Rev. **110**, 160 (1958).
[5] M. P. Nakada, J. D. Anderson, C. C. Gardner, and C. Wong, Phys. Rev. **110**, 1439 (1958).
[6] M. MacGregor, W. P. Ball, and R. Booth, Phys. Rev. **108**, 726 (1957).
[7] H. L. Taylor, O. Lönsjö, and T. W. Bonner, Phys. Rev. **100**, 174 (1955).
[8] W. P. Ball, M. MacGregor, and R. Booth, Phys. Rev. **110**, 1392 (1958).
[9] J. R. Beyster, M. Walt, and E. W. Salmi, Phys. Rev. **104**, 1319 (1956).
[10] D. W. Miller, R. K. Adair, C. K. Bockelman, and S. E. Darden, Phys. Rev. **88**, 83 (1952).
[11] M. Walt, R. L. Becker, A. Okazaki, and R. E. Fields, Phys. Rev. **89**, 1271 (1953).
[12] N. Nereson and S. Darden, Phys. Rev. **89**, 775 (1953).
[13] N. Nereson and S. Darden, Phys. Rev. **94**, 1678 (1954).
[14] A. Bratenahl, J. M. Peterson, and J. P. Stoering, Phys. Rev. **110**, 927 (1958).
[15] J. M. Peterson, A. Bratenahl, and J. P. Stoering, Phys. Rev. **120**, 521 (1960).
[16] M. H. MacGregor, W. P. Ball, and R. Booth, Phys. Rev. **111**, 1155 (1958).

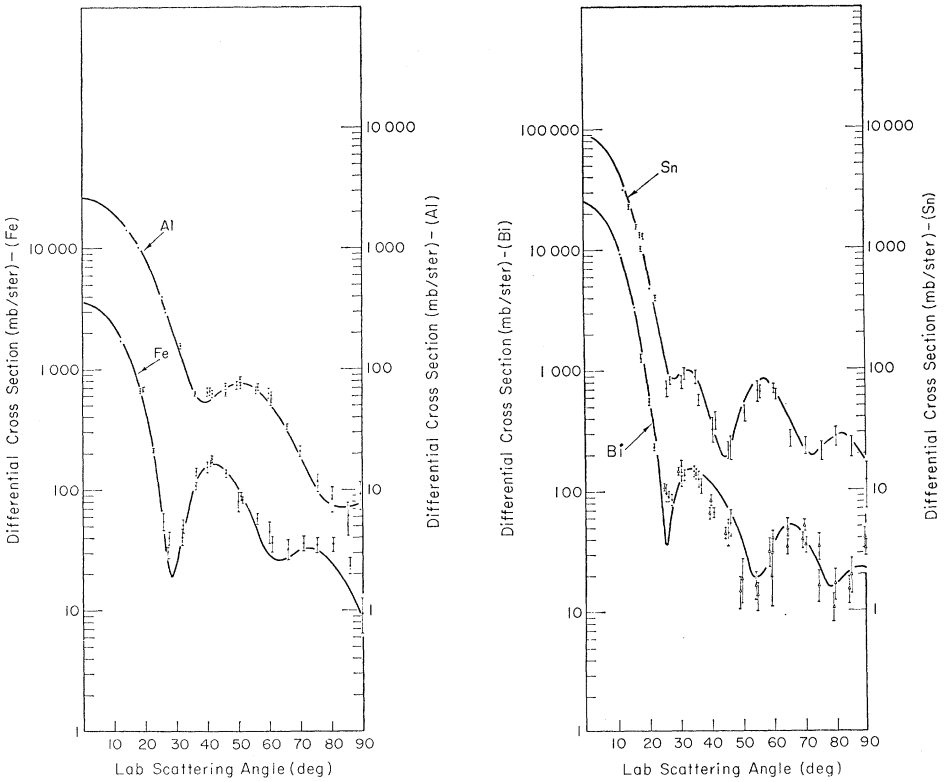

FIG. 3. Elastic scattering of 24-Mev neutrons by Al, Fe, Sn, Bi. Solid circles represent corrected data taken from scatterers $\frac{1}{2}$ total mean-free path in diameter; triangles, corrected data taken from scatterers $\frac{3}{4}$ total mean-free path in diameter. Solid lines are optical model predictions of Bjorklund and Fernbach.

fo two amplifiers. The output from one amplifier was ted to the input of an Argonne-type pulse-height analyzer; the output from the other amplifier was fed to four discriminator-gate units, which generated the gate pulses fed to the scalers and to the internal gate circuit in the pulse height analyzer. Scaler bias energies were set relative to the high end of the recoil proton spectrum. The bias adjustment was made by exposing the detector to the direct neutron flux and gating the pulse height analyzer with the outputs from the discriminator-gate units.

The above simplified electronics were employed only after ascertaining that time-of-flight techniques were not necessary. Time-of-flight experiments showed that the high detector biases used effectively eliminated the inelastic γ rays from the scatterer and the time-independent neutron-capture γ-ray background. These experiments also showed that the remaining background (measured with scatterer removed) arrived at the detector at the same time as the elastic neutrons. It is thus plausible that the residual background was due to neutron scattering from air and from the shielding.

III. MEASUREMENTS AND CORRECTIONS

Cross sections (uncorrected for effects due to scatterer size) were calculated from the following formula:

$$\frac{d\sigma}{d\omega}(\theta)=\frac{C_\theta}{C_0}\left(\frac{RD}{R+D}\right)^2\frac{\mathcal{E}(E_0)}{\mathcal{E}(E_\theta)}\frac{1}{N}, \quad (1)$$

where C_θ is the difference between the number of counts observed at an angle θ with scatterer in and the number of counts observed at the same angle with scatterer out; R is the distance between neutron source and scatterer; D is the distance between scatterer and detector; C_0 is the number of detector counts when source neutrons are viewed at a distance $R+D$ from the source along a line connecting source and scatterer; $\mathcal{E}(E)$ is the efficiency of the detector for neutrons of energy E; E_0 is the energy of the neutrons incident on the scatterer; E_θ is the energy of the neutrons elastically scattered through an angle θ by the scatterer; and N is the number of nuclei in the scatterer. The ratio of efficiencies $\mathcal{E}(E_0)/\mathcal{E}(E_\theta)$ was calculated from the bias energy, the shape of the recoil proton spectrum, total n-p cross section as a function of neutron energy, pulse height curves for the scintillator as a function of proton energy, and the kinematics of elastic scattering. Measurements of C_0 were made at reduced beam levels in order to minimize pileup effects.

Corrections for effects due to scatterer size such as multiple scattering, absorption, and angular resolution were calculated with a Monte Carlo code on the Univac and IBM 704. Corrected cross sections are shown in Fig. 3.

IV. ERRORS

The residual angular resolution of the corrected data is $\pm 2°$. Root-mean-square errors due to counting statistics are indicated by flags on the data points. Systematic errors are estimated at less than 5%.

The data points shown in Fig. 3 are those measured with the highest bias yielding reasonable counting statistics. This bias corresponds to a proton energy of 20 Mev. From the slope of the cross section vs bias curves it was estimated that, at the secondary maxima of the angular distributions, inelastic neutrons contribute less than 10%; at the minima on Sn and Bi, inelastic neutrons may contribute as much as 40%. In general, the percentage contribution of inelastic neutrons at the minima decreases with decreasing atomic weight.

To examine the effect of the shielding geometry upon cross sections near 90°, measurements were made between 60° and 90° both with and without the additional shielding shown as a cross-hatched area in Fig. 1. No difference between cross sections measured in the two geometries was observed, indicating the in-scattering correction is smaller than the counting statistics.

V. CONCLUSIONS

The optical model potential of Bjorklund and Fernbach has the following form[17]:

$$V(r,\boldsymbol{\sigma},\mathbf{l})=V_{CR}\rho(r)+iV_{CI}\exp[-(r-R)/b^2]+(V_{SR}+iV_{SI})(\hbar/\mu c)^2\frac{1}{r}\frac{\partial\rho(r)}{\partial r}\boldsymbol{\sigma}\cdot\mathbf{l}, \quad (2)$$

where $\rho(r)$ is the real potential form factor equal to $[1+\exp(r-R)/a]^{-1}$, μ is the π-meson mass, and $\boldsymbol{\sigma}$ and $\mathbf{l}$ are spin and orbital angular momenta of the incident particle in units of $\hbar$.

The following values were used in conjunction with the above potential to generate the angular distributions as shown in Fig. 3:

$$V_{CR}=40 \text{ Mev},$$
$$V_{CI}=11 \text{ Mev},$$
$$V_{SR}=7.4 \text{ Mev},$$
$$V_{SI}=0 \text{ Mev},$$
$$R=1.25A^{\frac{1}{3}}\times10^{-13} \text{ cm},$$
$$a=0.70\times10^{-13} \text{ cm},$$
$$b=1.00\times10^{-13} \text{ cm}.$$

Calculations of elastic scattering at angles less than 90° are insensitive to the magnitude of the spin orbit potential. Therefore the present measurements leave the spin-orbit potential largely undetermined. The above values of V_{SR} and V_{SI} were chosen on the basis of a fit[17] to back-angle elastic-neutron scattering at 14 Mev and proton polarization at 17 Mev. The above values of R, a, and b, to which the angular distributions are sensitive, are consistent with those[17–19] derived from measurements at other energies. With the use of these values, the measured angular distributions determine both real and imaginary potentials to ±1 Mev. In addition to giving the best fit to the angular distributions, the above values for the parameters generate total cross sections[15] and neutron nonelastic cross sections[16] in excellent agreement with measurements in this energy region.

ACKNOWLEDGMENTS

The authors extend grateful acknowledgements to M. Mansigh and R. M. Wright for programming the Monte Carlo calculations, to F. Bjorklund and S. Fernbach for optical model calculations, to J. M. Peterson for interest and encouragement during the course of the experiment, and to Hans Mark for illuminating discussions about the optical model.

[17] F. Bjorklund and S. Fernbach, *Exact Phase-Shift Calculation for Nucleon-Nuclear Scattering*, Proceedings of the Second International Conference on the Peaceful Uses of Atomic Energy, Geneva 1958, p. 649, Vol. 14, p. 24, United Nations, Geneva (1958).

[18] S. Fernbach, Revs. Modern Phys. **30**, 414 (1958).

[19] A. E. Glassgold, Revs. Modern Phys. **30**, 419 (1958).